Journal of Solid State Chemistry 183 (2010) 1090–1094

Contents lists available at ScienceDirect

Journal of Solid State Chemistry

journal homepage: www.elsevier.com/locate/jssc

Chemical route for formation of intermetallic Zn_4Sb_3 phase

A. Denoix, A. Solaiappan [1], R.M. Ayral *, F. Rouessac, J.C. Tedenac

Institut Charles Gerhardt Montpellier UMR 5253 (ICGM), C2M-UM2-CNRS, Pl. E. Bataillon, 34095 Montpellier Cedex 5, France

ARTICLE INFO

Article history:
Received 3 December 2009
Received in revised form
11 March 2010
Accepted 14 March 2010
Available online 18 March 2010

Keywords:
Solution synthesis
Zinc antimonide
Intermetallic
Solvent media

ABSTRACT

Synthesis of intermetallic zinc antimonide phases via low temperature solution route was investigated. Trial experiments were carried out under inert atmosphere at 70 °C using metallic Zn, $SbCl_3$ and $NaBH_4$ as reactants and tetrahydrofuran (THF), dimethylsulfoxide (DMSO) as organic media. Powder X-ray analysis confirmed the nucleation and growth of ZnSb phases in presence of excess Zn. SEM analysis revealed the existence of core–shell structure comprising of Zn core and Sb shell. Such particles get transformed into Zn_4Sb_3 crystalline phases upon thermal treatment at 300 °C/6 h in a silica tube closed under high secondary vacuum.

1. Introduction

Conversion of waste heat directly into useful electrical energy and vice versa is achieved by thermoelectric generators (TEG). They make use of 'Seebeck effect' in semiconducting materials. Development of reliable, low temperature operating TEG is becoming necessary today for converting the waste heat arising out of huge numbers of personal computers, high speed trains and automobiles and even from the domestic cooking ovens and hot plates [1]. In a typical TEG device, the conversion efficiency (η_{TE}) is proportional to a quantity called 'figure of merit' (ZT). For all the thermoelectric materials, ZT is theoretically defined as $ZT=(\alpha^2\sigma/k)T$, where σ and k are respective electrical and thermal conductivities and α is the Seebeck coefficient. It is mandatory for TEGs to have low thermal and high electrical conductivities for achieving high heat conversion efficiency. A target value of $ZT=4$ is recommended for low temperature operating TEGs [2].

Zinc antimonides are classical thermoelectric materials with the figure of merit value $ZT=\sim 1.3$ in the intermediate temperatures ($<400\,^{o}C$). The ZnSb and Zn_4Sb_3 are the potential zinc antimonide phases present in the Zn–Sb binary alloys system [3]. Three distinguished phases are identified in Zn–Sb system: ZnSb decomposing peritectically at 546 °C and Zn_4Sb_3 melting congruently at 563 °C. The stable ZnSb and Zn_4Sb_3 phases have been formed in between 150 and 494 °C. Presently, more attention is given for growing β-Zn_4Sb_3 due to its attractive low thermal conductivity ($k_{200-400\,^{\circ}C}=\sim 6\times 10^{-3}\,W\,cm^{-1}\,K^{-1}$) and density (6.07).

Zinc antimonide phases are synthesized, usually by melting the high purity metallic Zn and Sb powders taken in the mole ratio of 53:47 with 2–5 at% excess Zn, in an evacuated quartz ampoule followed by granulation and hot pressing [4,5]. Evaporation of molten zinc and antimony, in homogeneous microstructure, enlarged grain size, formation of undesirable phases (orthorhombic β-ZnSb and δ-Zn_4Sb_3), decomposition of Zn_4Sb_3 and cracking due to thermal expansion mismatch are the problems realized in fabrication of Zn_4Sb_3 materials. Processing methods such as direct hot pressing [6], mechanical alloying [7], pulse discharge sintering [8], sinter forging [9], spark plasma sintering [10], gradient freeze technique [11] and conventional solid-state ceramic route [12] followed by repeated cold rolling and annealing have been reported over the years.

Preparation of nano-Zn_4Sb_3 is emerging because it provides large numbers of active grain boundaries for phonon scattering and hence, a decrease in the bulk thermal conductivity [13]. Wet chemical routes are better known for their efficiency and easiness for controlling the particle size and morphology. To our knowledge, bulk synthesis of Zn–Sb intermetallic particles through chemical methods has not been reported. Only one study can be found in the literature: in that one, synthesis of nanostructured zinc antimonide was attempted by solution route [14]. First, the activated Zn and Sb nano particles were separately prepared from the respective chloride salts through redox reactions. Later, the chemically derived Zn, Sb nano particles were mixed and then heated to 200 °C under Ar atmosphere for prolonged hours to obtain the intermetallic Zn–Sb phases. We have recently initiated wet chemical synthesis of zinc

* Corresponding author.
E-mail address: rose-marie.ayral@univ-montp2.fr (R.M. Ayral).
[1] Permanent address: National Institute for Interdisciplinary Science and Technology [NIIST], CSIR, Trivandrum-695019, India.

0022-4596/$ - see front matter © 2010 Elsevier Inc. All rights reserved.
doi:10.1016/j.jssc.2010.03.024

antimonides with an aim to produce colloidal zinc antimonide dispersions. The present paper will study the synthesis of nano-Zn_4Sb_3 colloid and will show the different characterizations of this powder, including phase stability as a function of temperature using Raman spectroscopy.

2. Material and methods

Metallic Zn powder (99.99%, Good Fellow, USA), antimony trichloride (ACROS ORGANICS, USA), $NaBH_4$ (93%, TCI Europe, Belgium), Tetrahydrofuran (THF, 99.9%, Sigma-Aldrich, GmbH), dimethylsulfoxyde (DMSO) (Carlo erba reagents 99.5%) were used as reagents. Acetone (99%, Sigma-Aldrich, GmbH) was used for washing the precipitate. The Zn metal powder was stored in air tight container and preserved under argon for preventing the surface oxidation.

In a typical synthesis, Zn powder and $NaBH_4$ were first taken in a reflux flask fitted with the condenser. The flask was filled with high purity argon gas. The 80 mL THF were added and stirred under magnetic stirring. 10.5 mmol $SbCl_3$ was prepared separately in 20 mL THF. Zn:Sb molar ratio was fixed as 65:35 with Zn in excess.

The reaction temperature was maintained at 75 °C. After 30 min of stirring at this temperature, $SbCl_3$ solution was quickly injected. The reaction mixture suddenly turned black in color indicating the reduction of Sb^{3+} into metallic Sb according to the reaction (1):

$$9NaBH_4\ (sol)+3SbCl_3\ (sol)\rightarrow 3Sb\ (s)+9NaCl\ (s)+9BH_3\ (g)+Cl+9/2H_2\ (g)$$

The refluxing was continued at 75 °C/24 h. At the end, a black residue was collected and washed with excess THF followed by acetone. The powder was then dried under primary vacuum at 80 °C for 24 h.

The following treatments were done: first, using an other solvent (DMSO). This type of solvent allows increasing the temperature of the solution up to 190 °C, giving the opportunity to increase the diffusion rate inside the particles. Secondly, the obtained powder after THF synthesis was introduced into a silica tube sealed under secondary vacuum and heated at a temperature of 300 °C for 6 h.

In each case, the products were characterized by X-ray diffraction at $2\theta=20$–60° (XPert pro, Cu$K\alpha$ radiation, scanning step size 0.016° and step time 40 s). The morphology and composition of the precipitate were examined by transmission electron microscopy (TEM, JEOL 1200EXII 120 kV) and scanning electron microscopy (SEM, FEI Quanta 200) equipped with an energy dispersive X-ray spectroscopy (EDS). Raman spectroscopy (LabRAM-Isa – Dilor) was used to confirm results obtained by TEM and SEM. A Linkam TS1500 heating device designed to work from 50 to 1500 °C, adapted on the Raman spectrometer, was used for high temperature measurements in order to study the stability of the obtained nanopowder. The temperature was controlled by a thermocouple at the bottom of the crucible. Measurements were performed in argon through the silica windows from room temperature up to 350 °C. Each time a new temperature was reached, the sample was stabilized for a few minutes before acquisition. The spectra at high temperature were corrected for the thermal radiation background.

Finally, the product was characterized by Seebeck coefficient as a function of temperature.

3. Results and discussion

The preparation of ZnSb and Zn_4Sb_3 phases through conventional processes usually involves high reaction temperatures for melting the Zn and Sb metals. The given thermal energy, either externally supplied or generated in-situ as in the case of mechanical alloying, acts as main driving force for forming Zn, Sb solid solutions and inter-diffusion of atoms to achieve homogeneous intermetallic phase. Earlier studies report that once the Zn and Sb solid solutions are occurred, the nucleation and growth of ZnSb take place at a faster rate. Upon continuous aging at high temperatures, the Zn_4Sb_3 phase is achieved. Though the ZnSb phase is formed quickly, the transformation of ZnSb into Zn_4Sb_3 reaction is more sluggish even at elevated temperatures. The reaction kinetics is very critical and a slight variation even in the stoichiometry as well as in thermal gradients caused decomposition of Zn_4Sb_3 into ZnSb and also formation of metastable zinc antimonide phases [15].

The solution route is entirely different from the conventional thermal processes and, therefore the involved reaction mechanism is also quite different. In solution route, factors such as initial molar concentration, polarity and pH of the reaction medium, enthalpy of the reactants, and diffusivity of the solute ions at the given reaction temperatures and time are deciding the reactivity, nucleation and growth of the desired phases.

In our case, the complete dissolution of antimony precursor in the given reaction medium THF, is first wetting the metallic zinc surface. The $SbCl_3$ is attacked by both Zn metal and $NaBH_4$ reductant. At this condition, the completely dissolved antimony chloride ions interact with Zn at molecular scale and form reactive Sb-nuclei and get deposited over the metallic Zn powders finally forming a coating. The Zn powder acts as a substrate for the growth of Sb structures. Such nano-Sb has high surface energy and therefore reacts readily with Zn for forming ZnSb nuclei. In fact, we tested the reduction of $SbCl_3$ using Zn powder without any $NaBH_4$. We have seen from the powder-X-ray analysis that there is only Sb and Zn peaks. It confirms that for accelerating the reaction kinetics primary reductant such as $NaBH_4$ is required and the excess Zn can act only as secondary reducing agent. The reaction temperature was purposefully controlled below 70 °C. In these conditions, the obtained product was analyzed by X-ray diffraction and only peaks belonging to Zn and Sb phases were evidenced (Fig. 1). The first step of our procedure consisting of reduction of $SbCl_3$ into Sb was successful. In order to enhance reactivity, DMSO was added to the solution which was heated to 180 °C. Fig. 2 shows XRD pattern of the resultant products using THF medium plus DMSO at 180 °C. All the diffraction peaks can be indexed and correspond to metallic Sb and Zn phases and Zn_4Sb_3 phase. The peaks at $2\theta=28.8^\circ$, 40.24° and 42.1° represent

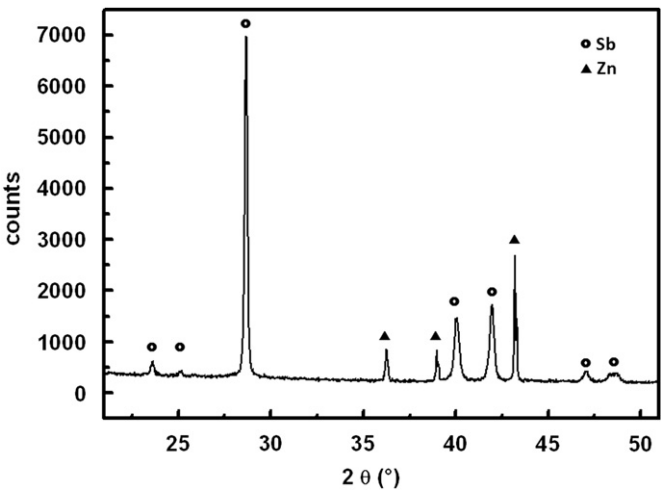

Fig. 1. X-ray diffraction pattern of the product directly obtained by the chemical route in THF medium.

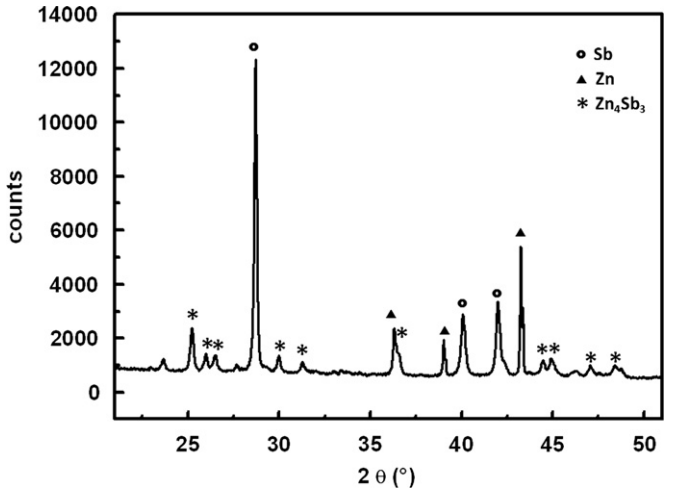

Fig. 2. X-ray diffraction pattern of the product directly obtained by the chemical route in THF+DMSO media.

rhombohedral Sb phase. The major Zn_4Sb_3 peaks corresponding to (300), (113) and (122) crystal planes are clearly noticed. These results show that an increase of temperature inside the reactor by means of the use of DMSO is determinant in formation of Zn_4Sb_3 phase. In order to understand the mechanism of formation obtained by chemical route, the powders were polished and then, observed by scanning electron microscopy. The distributions of Sb and Zn at% from core to the shell were also examined. The chemical compositions from surface to core are plotted (Figs. 3a and b). The composition of the outer shell is Sb phase rich and when we approach towards core only a rich Zn is present. Formation of the binary phase can occur at the interface between zinc core and antimony shell.

The analysis of the powder by Raman spectroscopy was made in different zones corresponding to the interface between the core and the shell and one corresponding to the shell (Figs. 4a and b). Three peaks are easily observable in the Raman spectrum of the powder: the peak at $175\,cm^{-1}$ undoubtedly corresponds to β-Zn_4Sb_3 phase. Whereas, the one at $115\,cm^{-1}$ to Sb phase and the peak at $152\,cm^{-1}$ to both Sb and Zn_4Sb_3 phases. Zn phase cannot be evidenced by Raman spectroscopy using this device because the characteristic line of Zn phase is observable at $<50\,cm^{-1}$. The powder particle is composed of a core–shell structure in which the core is constituted by intermetallic phase and the shell by antimony.

Ageing at 300 °C for 6 h in an evacuated quartz ampoule was carried out on the THF treated powder. XRD examination (Fig. 5) shows the absence of Sb and/or Zn peaks as well as ZnSb ones. All peaks in the pattern correspond to the reflections of rhombohedral phase Zn_4Sb_3 which are in agreement with the cell parameters, $a=12.233$ Å, $c=12.428$ Å. The ageing at 300 °C for 6 h was good enough to give rise to an inter-diffusion of antimony and zinc in order to elaborate the pure phase Zn_4Sb_3. XRD can be used to evaluate peak broadening with crystallite size. Scherer formula [16] $D=k\lambda/\beta_{hkl}\cos\theta$, where D is the crystallite size, k is the shape factor (0.9), λ is the wavelength of Cu$K\alpha_1$ radiation β_{hkl} is the instrumental corrected integral breadth of the reflection (in radians) located at 2θ and θ is the angle of reflection (in degrees) was utilized to relate the crystallite size to the line broadening. The instrumental corrected broadening β_{hkl} corresponding to the diffraction peak of Zn_4Sb_3 was estimated by using the relation $\beta_{hkl}=[(\beta_{hkl})^2-\beta^2_{\text{instrumental}}]^{1/2}$. The average crystallite size of the Zn_4Sb_3 nanoparticles was found to be 60 nm.

SEM observations (Fig. 6) of the powder show an agglomeration of grains of approximately 20 μm, which are

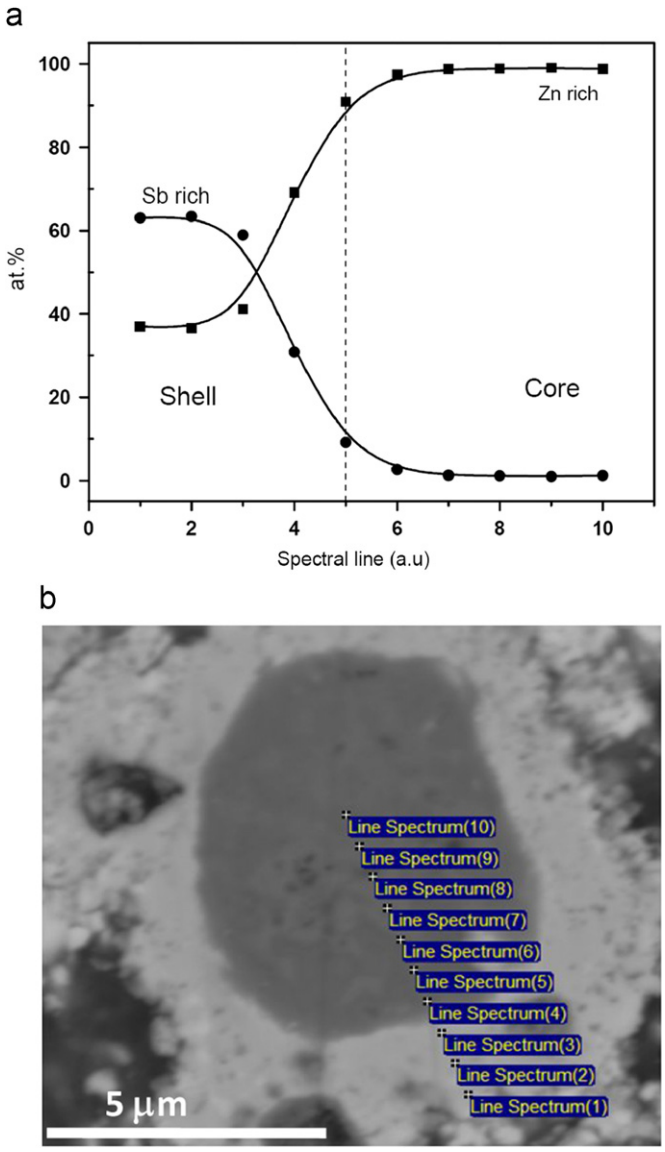

Fig. 3. EDX analysis and chemical composition of the Zn core and Sb shell (a curve indicating the distribution of atomic wt% of Zn and Sb in core and shell b: Microstructure and ED scanning positions of the particle from core to shell. Data taken for plotting the curve).

composed of particles not higher than a nanometer. Fig. 7 shows a typical TEM image of the powder de-agglomerated by ultrasonicator. It can be seen from this figure that the powder is uniform and consists of nanoparticles with average particle size of 20 nm.

The analysis of the powder by Raman spectroscopy was made in different random zones (Fig. 8) at 25 °C. Three peaks (*) are easily observable in the Raman spectrum of the powder: 155, $175\,cm^{-1}$ and one between 320 and $330\,cm^{-1}$, all of them correspond to β-Zn_4Sb_3 phase. This result is in agreement with the XRD analysis. In this spectrum, the peak at $115\,cm^{-1}$ which undoubtedly corresponds to Sb phase does not appear. We obtain a pure intermetallic phase of β-Zn_4Sb_3 due to complete diffusion of Zn and Sb during the ageing at 300 °C.

Zn_4Sb_3 formation mechanism can be divided into three steps such as wetting of Zn metal surface by molecular scale $SbCl_3$ precursor solution, reduction of $SbCl_3$ into Sb nuclei and growth of Sb nuclei over the surface of Zn to form a core–shell Zn–Sb particles and finally transformation into Zn_4Sb_3 phase when

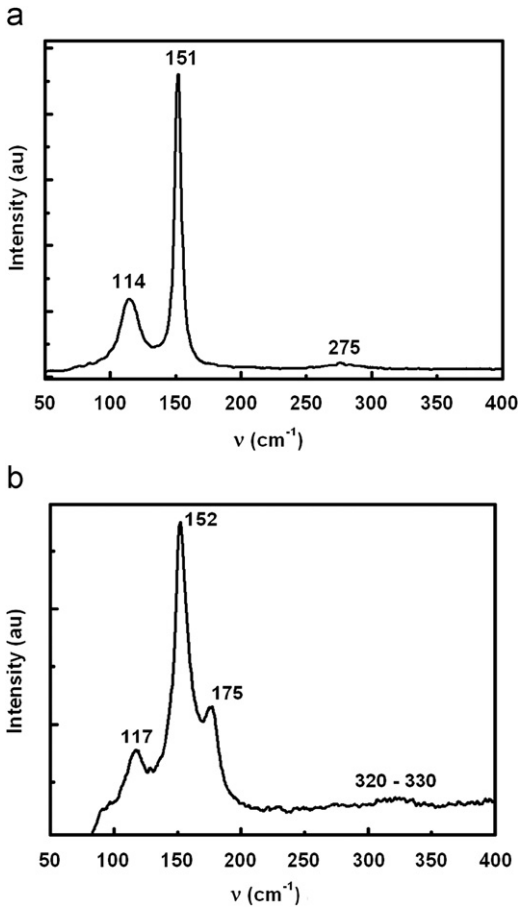

Fig. 4. (a) Raman spectroscopy of the shell structure (Sb evidenced) and (b) Raman spectroscopy of a particle Zn_4Sb_3 phase evidenced.

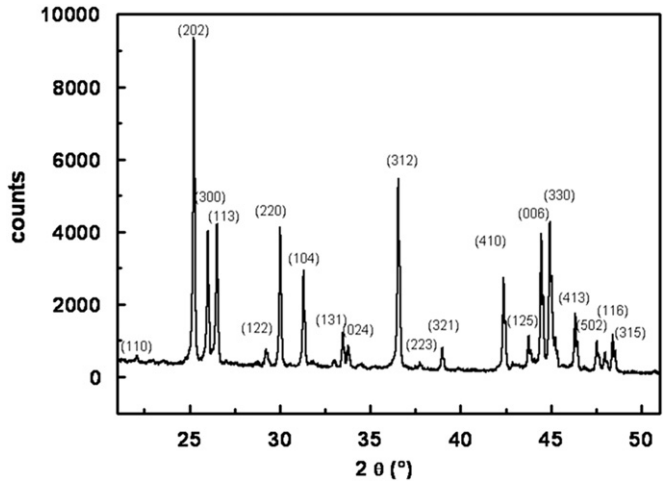

Fig. 5. X-ray diffraction pattern of the product obtained by the chemical route in THF media and after ageing in an evacuated quartz ampoule at 300 °C for 6 h.

DMSO used at 180 °C. We have clearly seen the formation of Zn core and Sb shell morphology from the SEM analysis. Such core–shell precursor's nature is highly favorable for the accelerated diffusion. In core–shell particles, the diffusion path is less and therefore the mass transfer takes place even at low reaction temperatures. In our case, annealing at 300 °C for 6 h gave rise to the formation of Zn_4Sb_3 phase into the powder.

Fig. 8 shows Raman spectra obtained in situ at four different temperatures: 25, 200, 350 °C and finally back to room

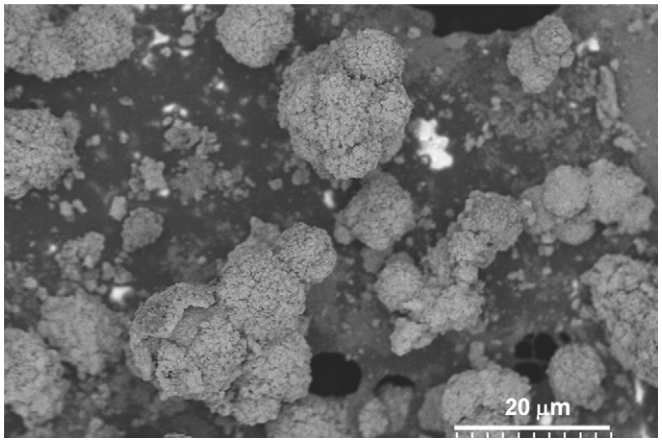

Fig. 6. SEM observation of the synthesized powder.

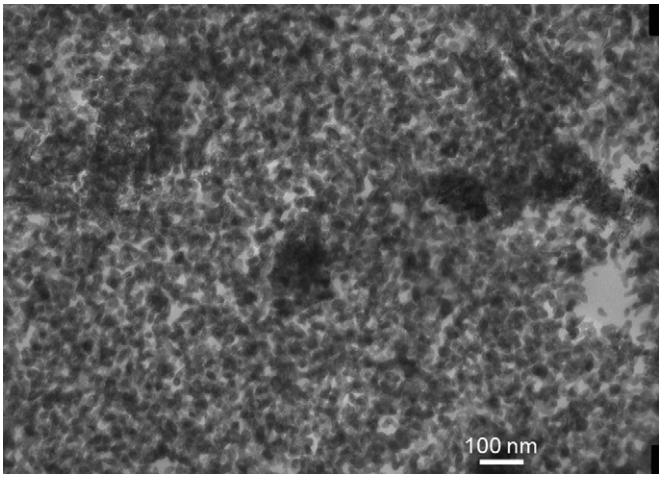

Fig. 7. TEM observation of the powder.

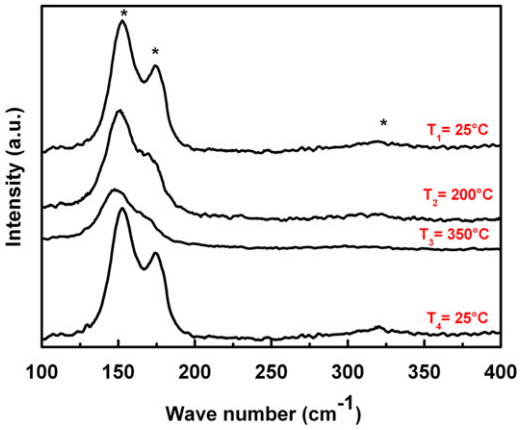

Fig. 8. Raman spectroscopy of the product obtained by chemical route in THF media and after ageing in an evacuated quartz ampoule at 300 °C for 6 h at different temperatures.

temperature 25 °C. For each temperature, the sample was stabilized for 10 min before recording the spectrum. Very few changes are induced by temperature up to 350 °C apart from a progressive broadening of the bands and a weak peaks shift to left as temperature increased. It is interesting to note that, at

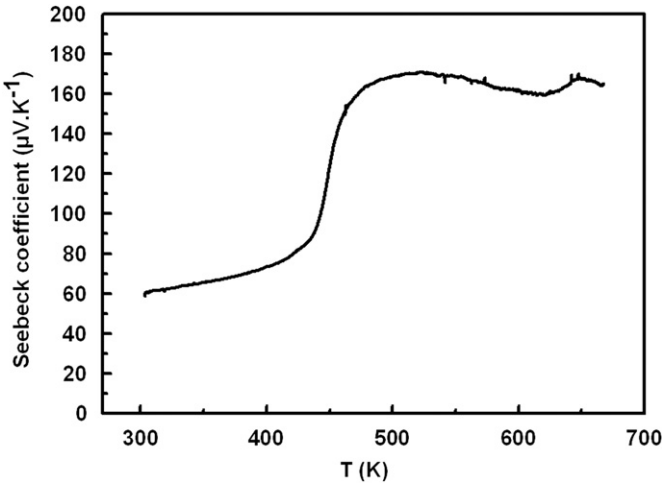

Fig. 9. Temperature dependence of Seebeck coefficient as a function of temperature.

T_4=25 °C, after thermal treatment, only vibrations corresponding to Zn_4Sb_3 phase are evidenced. This result evidences the thermal stability of nano-Zn_4Sb_3 phase until 350 °C.

Seebeck coefficient measurements as a function of temperature in the range 25–425 °C were realized on these powders compacted under a pressure of 55.5 MPa without any sintering to avoid grains growth with temperature. The sample is placed in a furnace heated at 50 °C/h up to 400 °C under primary vacuum. Fig. 9 shows the temperature dependence of Seebeck coefficient: it increased from 60 to 170 μV/K at 325 °C. This value is similar to the result of Zn_4Sb_3 reported by Caillat et al. [4].

4. Conclusions

Synthesis of zinc antimonide intermetallic particles has been attempted for the first time through low temperature reduction reaction using metallic zinc and $SbCl_3$ as reactants and $NaBH_4$ as reducing agent in organic solvents, THF and DMSO. The process initially yielded core–shell ZnSb particles that get transformed into mixture Zn_4Sb_3 phase upon thermal treatment at 300 °C/6 h in a silica tube under secondary vacuum. The obtained powder was then characterized by SEM and TEM and was composed of nanosized-grains. Now the study in progress is to characterize it from a thermoelectric point of view.

Acknowledgments

The authors would like to thank ANR-07-Nano-021-02'Nano-microstil'for its financial support.

References

[1] A. Weidenkaff, R. Robert, M. Aguirre, L. Bocher, T. Lippert, S. Canules, Renewable Energy 33 (2008) 342–347.
[2] T.M. Tritt, M.A. Subramanian, MRS Bull. 31 (2006) 188.
[3] J.B. Li, M.C. Record, J.C. Tedenac, J. Alloys Compd. 438 (2007) 171–177.
[4] T. Caillat, J.-P. Fleurial, A. Borshchevsky, J. Phys. Chem. Solids 58 (1997) 1119–1125.
[5] T.J. Zhu, X.B. Zhao, M. Yan, S.H. Hu, T. Li, B.C. Zhou, Mater. Lett. 46 (2000) 44–48.
[6] S.C. Ur, I.H. Kim, P. Nash, Mater. Lett. 58 (2004) 2132–2136.
[7] V. Izard, M.C. Record, J.C. Tedenac, J. Alloys Compd. 345 (2002) 257.
[8] T. Itoh, J. Shan, K. Kitagawa, J. Prop. Pow. 24 (2008) 353.
[9] S.C. Ur, P. Nash, I.H. Kima, Mater. Lett. 58 (2004) 2937–2941.
[10] T. Souma, G. Nakamoto, M. Kurisu, J. Alloys Compd. 340 (2002) 275–280.
[11] G. Nakamoto, N. Akai, M. Kurisu, J. Alloys Compd. 437 (2007) 151–156.
[12] S.C. Ur, P. Nash, I.H. Kim, J. Alloys Compd. 361 (2003) 84–91.
[13] A. Weidenkaff, R. Robert, M.H. Aguirre, L. Bocher, L. Schlapbach, Phys. Status Solidi 6 (2007) 247–249.
[14] S. Schlecht, C. Erk, M. Yosef, Inorg. Chem. 45 (2006) 1693–1697.
[15] K. Ueno, A. Yamamoto, T. Noguchi, T. Inoue, S. Sodeoka, H. Takazawa, C.H. Lee, H. Obara, J. Alloys Compd. 384 (2004) 254–260.
[16] J.I. Langford, A.J.C. Wilson, J. Appl. Crystallogr. 11 (1978) 102.